# Sliding Wear Properties of HVOF Sprayed WC-10Co4Cr Coatings With Conventional Structure and Bimodal Structure Under Different Loads

**Yong-Kuan Zhou**
School of Engineering and Technology,
China University of Geosciences (Beijing),
Beijing 100083, China
e-mail: yongkuanz@163.com

**Jia-Jie Kang**[1]
School of Engineering and Technology,
China University of Geosciences (Beijing),
Beijing 100083, China;
State Key Laboratory of Tribology,
Department of Mechanical Engineering,
Tsinghua University,
Beijing 100084, China;
Zhengzhou Institute,
China University of Geosciences (Beijing),
Zhengzhou 451283, China
e-mail: kangjiajie@cugb.edu.cn

**Wen Yue**
School of Engineering and Technology,
China University of Geosciences (Beijing),
Beijing 100083, China;
Zhengzhou Institute,
China University of Geosciences (Beijing),
Zhengzhou 451283, China
e-mail: cugbyw@163.com

**Xiao-Bin Liu**
School of Engineering and Technology,
China University of Geosciences (Beijing),
Beijing 100083, China
e-mail: 18689840761@163.com

**Zhi-Qiang Fu**
School of Engineering and Technology,
China University of Geosciences (Beijing),
Beijing 100083, China;
Zhengzhou Institute,
China University of Geosciences (Beijing),
Zhengzhou 451283, China
e-mail: fuzq@cugb.edu.cn

**Li-Na Zhu**
School of Engineering and Technology,
China University of Geosciences (Beijing),
Beijing 100083, China;
Zhengzhou Institute,
China University of Geosciences (Beijing),
Zhengzhou 451283, China
e-mail: zhulina@cugb.edu.cn

**Ding-Shun She**
School of Engineering and Technology,
China University of Geosciences (Beijing),
Beijing 100083, China;
Zhengzhou Institute,
China University of Geosciences (Beijing),
Zhengzhou 451283, China
e-mail: shedingshun@163.com

**Guo-Zheng Ma**[1]
National Key Lab for Remanufacturing,
Academy of Armored Forces Engineering,
Beijing 100072, China
e-mail: magz0929@163.com

**Hai-Dou Wang**
School of Engineering and Technology,
China University of Geosciences (Beijing),
Beijing 100083, China;
National Engineering Research Center for Remanufacturing;
National Key Lab for Remanufacturing,
Academy of Armored Forces Engineering,
Beijing 100072, China
e-mail: wanghaidou@aliyun.com

*The WC-10Co4Cr coatings with conventional structure and bimodal structure were sprayed by high-velocity oxygen fuel (HVOF) technology. The phase compositions and morphologies of the WC-10Co4Cr powders and coatings were analyzed by X-ray diffraction (XRD) and scanning electron microscopy (SEM). The microhardness, porosity, bonding strength, elastic modulus, and indentation fracture toughness of the conventional coating (Conventional) and the bimodal coating (Bimodal) were also studied. The sliding wear properties of the Conventional and the Bimodal against $Si_3N_4$ counterballs under different loads at room temperature (~25 °C) were investigated using a friction and wear tester. Compared with the Conventional, the Bimodal has denser microstructure, lower porosity, more excellent mechanical properties, and the Bimodal has better wear resistance than the Conventional under different loads. The two coatings under 15 N and 30 N only exhibit abrasive and slightly adhesive wear mechanism, while in the load application of 45 N, additional mechanism which is fatigue is detected and causes flaking of the coating.*
[DOI: 10.1115/1.4050735]

*Keywords: HVOF, WC-10Co4Cr coating, conventional, bimodal, sliding wear*

## 1 Introduction

Tungsten carbide (WC)-based cermet thermal spray coating has been widely used in aviation, power, metallurgy, petroleum, chemical, machinery, and other industrial fields due to its excellent wear resistance [1–3]. Research shows that the mechanical properties of the coating depend on its porosity, bonding state between particles, and phase structure [4,5]. Compared with other thermal spray technologies, high-velocity oxygen fuel (HVOF) has high particle velocity, low flame temperature, and short flying time of sprayed particles in the air, which can significantly shorten the residence time of the WC particles in the flame stream and reduce the

[1]Corresponding authors.

Contributed by the Tribology Division of ASME for publication in the Journal of Tribology. Manuscript received November 13, 2020; final manuscript received March 26, 2021; published online April 19, 2021. Assoc. Editor: Jun Qu.

  

degree of decarburization of the WC particles. Therefore, the prepared coating is denser, which is helpful to improve the wear resistance and the binding force between particles of the coating [6–9].

As one of the three main failure forms of materials, wear is the process of material transfer and loss in the relative movement of the contact surface of materials [10,11]. Several studies have explored that the wear properties of the WC-based cermet coatings depend on several factors such as the initial powder morphology, the carbide particle size, and distribution in the binder phase [12,13]. As a result, nanostructured WC ceramic coatings deposited by HVOF have been studied to improve the sliding wear resistance of the coatings [3,14–16]. However, decarburization will intensify as the size of carbide decreases during the spraying process, resulting in increased brittleness of the coating and reduced the wear resistance. Therefore, the production of bimodal powder can not only maintain the enhanced properties but also reduce the decarburization. This powder contains two kinds of WC particles of microstructure and nanostructure [17–20].

The wear resistance of the coating is functionally related to the hardmetal plane strain bulk fracture toughness. As the fracture toughness increases, the wear resistance increases. The fracture toughness of the WC ceramic coating increases with the increase of average size of carbide grain, volume fraction of binder phase, and mean free path. In general, since the invention of cemented carbide, the simultaneous improvement of toughness and hardness has been a major research direction [21,22]. It is reported that the developed bimodal coating has good wear properties for its good combination of WC microparticles and nanoparticles [23]. Besides, the sliding wear behaviors of the WC-based cermet coatings at different conditions are different, so the test conditions are critical to the wear behavior of the coating, such as the load applied on the sample, the sliding wear speed, and the experimental temperature [3].

Previous work has reported the wear behavior of conventional coatings, but there is few research on bimodal coatings, especially the comparison of the wear behavior of the two coatings under different load conditions. In this study, the WC-10Co4Cr coatings with conventional structure and bimodal structure were sprayed by HVOF technology. The phase compositions, microstructure, microhardness, porosity, bonding strength, and indentation fracture toughness of both coatings were analyzed. Besides, a series of sliding wear tests under different loads at room temperature were conducted to research the wear behaviors of the conventional coating (Conventional) and the bimodal coating (Bimodal). The conventional structure refers to the structure containing micro-scale WC particles, while the bimodal structure refers to the structure containing nano-scale and micro-scale WC particles in a ratio of 3:7. In the following, the Conventional is used to represent the conventional coating, and the Bimodal is used to represent the bimodal coating.

## 2 Experimental Procedure

**2.1 Sample Manufacturing.** AISI 4135 steel with a size of 40 mm × 25 mm × 5 mm was chosen as the substrate, and the chemical composition of AISI 4135 steel was as follows: C: 0.18–0.40, Si: 0.17–0.37, Mn: 0.40–0.70, Cr: 0.80–1.10, and balance Fe. Two kinds of WC-10Co4Cr powders (provided by BGRIMM Technology Group, which is located in Beijing, China) were prepared by agglomeration and sintering. The proportion of the two powder components is the same: WC-86 wt%, Co-10 wt%, and Cr-4 wt%. According to the size of the WC particles, the WC-10Co4Cr powders can be divided into conventional powders and bimodal powders. The WC particles are micro-scale (0.7–1.5 $\mu$m) in the conventional powders, and WC particles are a mixture of nano-scale (70–200 nm) and micro-scale (0.2–1.3 $\mu$m) in the bimodal powders. The two powders were used as raw materials for HVOF spraying.

The substrate surfaces were degreased and sandblasted before the spraying process in order to increase the bond strength between the coating and substrate [24] using corundum with a size of 0.3 mm as the blasting material. The blasting distance was 300 mm, and the angle was 70 deg. Then, AISI 4135 steel substrate was placed in an ultrasonic machine and cleaned with ethanol for 30 min. In addition, in order to obtain tightly bonded coatings during the spraying process, the substrate was placed in a drying oven (Lichen, 101-0BS; China) and preheated at 150 °C.

The Conventional and the Bimodal were sprayed by HVOF technology (GTV Impex GmbH, Germany) equipped with GTV HVOF K2 spray gun. The thickness of the prepared coating was about 250 $\mu$m. Nitrogen was used as the carrier gas. The HVOF spraying parameters of WC-10Co4Cr coatings are shown in Table 1.

**2.2 Microstructural Characterization.** The morphologies of the powders and the coatings were investigated by ZEISS MERLIN Compact scanning electron microscope (SEM). And the composition of the coatings was analyzed by energy dispersive spectroscopy (EDS). Porosity of the coatings was measured by the IMAGEJ2X software based on the cross-sectional images (500×). The phase composition of the powders and the coatings was observed by Brunker AXS D-8 X-ray diffraction (XRD) operated with Cu Kα radiation. The scanning speed is 4 deg/min, and the range of $2\theta$ is 20–90 deg. Quantitative analysis of phase content was measured by the reference intensity ratio (RIR) method. The phases in the powders and the coatings were analyzed using the MDI JADE 6.0 software.

According to the standard ASTM C633, the bond strength between the coating and the substrate was measured with a universal tensile test equipment (Instron 5985, United States) at a tensile rate of 1 mm/min, and the averaged five experimental data were taken as the test result. The microhardness of the coatings was determined by a Buehler MICROMET-6030 microhardness tester under a load of 300 g for 15 s (ten measurement points on the cross section). The elastic modulus of the coatings was measured by Agilent Nano Indenter G200 with a load of 300 g for 20 s, and takes the value of ten tests as the average elastic modulus. The indentation fracture toughness ($K_{IC}$) was measured through the Vickers hardness tester (200HV-5; Lailuote, China). The applied load was 49 N, and the dwell time was 15 s. The effective indentation fracture toughness value was the average of 20 measurements.

The fracture toughness of the coatings is calculated according to the Evans and Wilshaw model using the following equation [25]:

$$K_{IC} = \frac{0.079P}{a^{\frac{3}{2}}} \lg\left(\frac{4.5a}{c}\right) \tag{1}$$

where $P$ (N) represents the load applied to the indenter, $a$ (m) is half of the diagonal length of the Vickers indentation, and $c$ (m) is the crack length of the indentation. The equation requires the $c/a$ ratio should be in a range of 0.6–4.5.

**2.3 Tribology Tests.** The coatings prepared by HVOF were polished to make the roughness $Ra \leq 0.8$ $\mu$m, to prevent great fluctuation of the coefficient of friction (COF). The wear resistance of the two coatings was tested by Brunker CETR-UMT-3 friction and wear testing machine. The $Si_3N_4$ ball with a diameter of 12.7 mm was chosen as the counterball because it is harder than the WC-10Co4Cr coating, and it has been used in many friction and wear studies of WC-based coatings [26,27]. The sliding wear tests lasted for 30 min utilizing a stroke length of 5 mm, a frequency of 10 Hz, and a sliding speed of 0.2 m/s. This corresponded to a total sliding distance of 360 m. Wear tests were tested at room

**Table 1 High-velocity oxygen fuel spraying parameters of WC-10Co4Cr coatings**

| Oxygen flowrate | Spray distance | Powder feed rate | Kerosene flowrate | Nitrogen flowrate | Spray speed |
|---|---|---|---|---|---|
| 902 l/min | 420 mm | 100 g/min | 26 l/h | 9 l/min | 0.5 m/s |

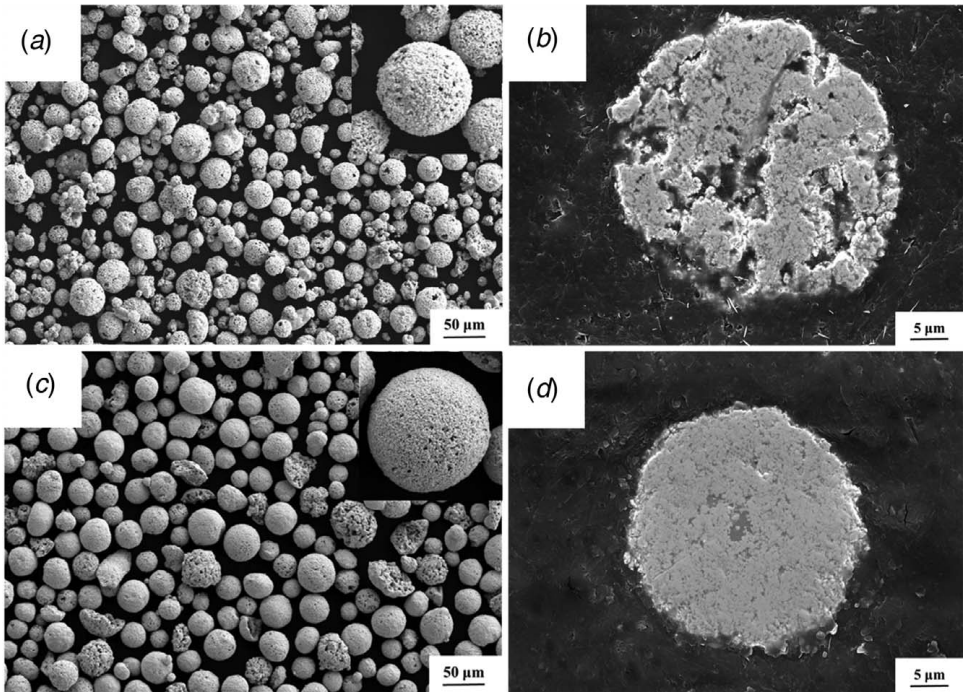


**Fig. 1 Electron microscopy images of WC-10Co4Cr powders: (*a*) the overall morphology of the conventional powders, (*b*) the cross-sectional of the conventional powders, (*c*) the overall morphology of the bimodal powders, and (*d*) the cross-sectional of the bimodal powders**

temperature (~25 °C). The wear volume was integrated from the confocal outline of the Zygo NexView three-dimensional instrument. The wear-rate was calculated by the following equation [28]:

$$Q = \frac{V_W}{NS} \tag{2}$$

where $Q$ is the wear-rate ($mm^3/(N\,m)$), $V_W$ is the wear volume ($mm^3$), $N$ represents the applied load (N), and $S$ refers to total sliding distance (m).

In order to examine the sliding wear behavior of the coatings and the uncoated substrate under different loads, the loads on the coatings were set as 15 N, 30 N, and 45 N and the other wear conditions were kept constant. Each experiment was repeated for three times to ensure the stability of the wear data. In order to compare the wear resistance of the coatings, the friction and wear test of the uncoated substrate was carried out under the same condition.

## 3 Results and Discussion

**3.1 Coating Characterization.** Figures 1(*a*) and 1(*c*) show two kinds of powders made by agglomeration and sintering. They show spherical morphologies with dense structures, thus the powders have good fluidity. But compared with conventional powders, the bimodal powders have smoother surfaces and denser structures. This phenomenon is also reflected on the cross-sectional of the powders in Figs. 1(*b*) and 1(*d*). The nano-scale WC particles fill the pores of micro-scale WC particles, so the bimodal powders have denser internal structure and fewer pores.

The representative SEM cross-sectional images of HVOF sprayed coatings are shown in Fig. 2. As is seen in Figs. 2(*a*) and 2(*c*), there are no obvious defect at the interface between the coating and the substrate of the Conventional and the Bimodal. The interface between the coating and the substrate is well bonded, and the thickness of the coatings is about 250 $\mu$m. There are some pores in the internal of the coatings, but the Bimodal has better microstructure. The main reason is that the nanostructured WC particles are distributed in overall coatings dispersedly, which plays the role of dispersion strengthening [4]. As is seen in Figs. 2(*b*) and 2(*d*), the WC-10Co4Cr coatings consist of two phases: WC hard phase embedded in CoCr binder phase. Figures 2(*e*) and 2(*f*) show the as-deposited surface of the two coatings. It can be seen that the surface of both coatings is rough, but the Conventional has more unmelted particles. Besides, the porosity measured by image analysis (gray method) was $2.0\% \pm 0.1$ for the Conventional and $1.4\% \pm 0.1$ for the Bimodal, respectively. There are a large number of coarse WC particles and a small part of fine WC particles and some pores in the Conventional. These fine WC particles are caused by the rupture of coarse-grained WC caused by the high-speed collision during the HVOF spraying process [29]. However, in the Bimodal, the microstructure is denser and the porosity is lower compared with the Conventional due to the mixture of nano-scale and micro-scale WC particles and the CoCr binder phase is filled between the WC particles. As is seen in Figs. 2(*g*) and 2(*h*), Co element is mainly distributed around WC particles, while the distribution difference of Cr element is not obvious due to its low content.

Figure 3 presents the XRD patterns of the WC-10Co4Cr powders and coatings. As is seen in Figs. 3(*a*) and 3(*b*), the main phase of the two powders is WC phase, and a small amount of Co and $Co_xW_yC$ ($Co_3W_3C$, $Co_6W_6C$, etc) also exist [30]. During the sintering of WC-10Co4Cr powder, the CoCr binder reacted with the WC particle phase to form the $Co_xW_yC$. In Figs. 4(*c*) and 4(*d*), both coatings contain WC and a few $W_2C$ phases, indicating that some WC phases were decarburized during the HVOF spraying process [2,31,32]. The content of $W_2C$ in the Conventional and the Bimodal is 3.06% and 4.52% by the RIR method. The Bimodal is more likely to decarburize due to larger specific surface area of WC particles. However, Co was converted to amorphous phase or nanocrystalline of binder phase, and thus, the diffraction peak of Co phase do not exist in the XRD patterns of the coatings [33,34].

The mechanical properties of the coatings are summarized in Table 2. Both coatings have good bonding strength. Compared with the Conventional, the Bimodal has higher average microhardness and elastic modulus, but the indentation fracture toughness is

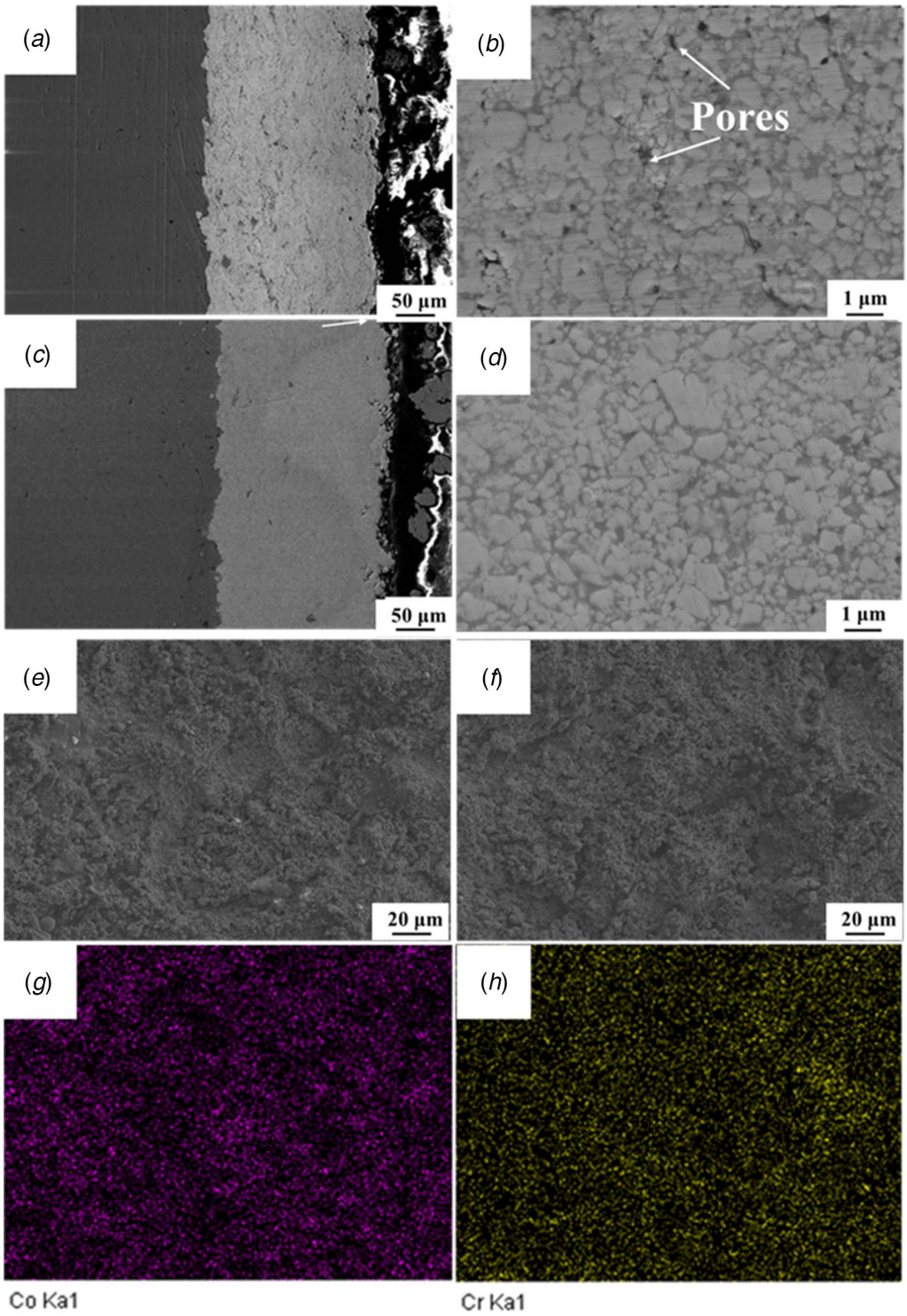


**Fig. 2 Cross-sectional of the WC-10Co4Cr coatings: (*a*) the overview of the Conventional, (*b*) the high magnification of the Conventional, (*c*) the overview of the Bimodal, (*d*) the high magnification of the Bimodal, (e) as-deposited surface of the Conventional, (*f*) as-deposited surface of the Bimodal, (*g*) Co distribution in (*d*), and (*h*) Cr distribution in (*d*)**

basically the same. And based on previous studies, the microhardness of the coatings is about four times than that of the uncoated substrate [8]. In the Bimodal, the nano-scale WC particles are uniformly distributed around the micro-scale WC particles, which plays the role of dispersion strengthening. Besides, according to the Hall–Petch relationship, the microhardness of the coatings decreases with increasing the WC grain size [35]. The addition of nano-grains into microstructures increased hardness without sacrificing indentation fracture toughness.

**3.2 Tribological Behavior of the Coatings.** The COF curves of the coatings and the uncoated substrate under different loads are shown in Fig. 4. At the beginning of the sliding wear, the COF

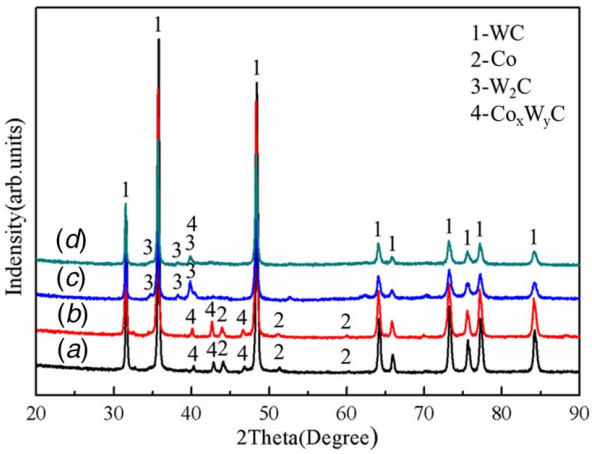


**Fig. 3 XRD patterns of the WC-10Co4Cr: (*a*) the conventional powder, (*b*) the bimodal powder, (c) the conventional coating, and (*d*) the bimodal coating**

increases sharply with time. This is because that there is a micro-convex body on the contact surface between the coating and counterball, resulting in a small contact area. With continuous wear, the contact area of the coating and counterball gradually increases, the increasing load are flattened and the COF decreases, and then the sliding wear enters a steady-state. During the steady-state wear, the counterball first wears the CoCr binder phase in the coating, and the WC particles are exposed to hinder the relative sliding, leading to an increase in the COFs. When the WC particles are exfoliated, the friction force is reduced, and the corresponding COF is dropped, and therefore, the COF still fluctuates up and down within a certain range.

For the effect of load on the COF of the coatings, the Conventional and the Bimodal have shown similar trends that the COF decreases with increasing load. In general, a lower COF means a higher wear resistance [36]. This is because that the thermal effect of friction is more significant as the load increases, and the generated oxidation products have a certain friction reduction effect [16,26]. Furthermore, the fluctuation range of the COF decreases as the load increases, which is attributed that the penetration depth of the counterball raises with the load increasing, and the peeling interval of the binder phase and WC hard particles is shortened. The wear tracks are relatively flat, and the fluctuation of the COF is reduced.

**Table 3 Average COF value of the coatings and the uncoated substrate under different loads**

| | 15 N | 30 N | 45 N |
|---|---|---|---|
| Conventional | $0.446 \pm 0.029$ | $0.377 \pm 0.019$ | $0.288 \pm 0.013$ |
| Bimodal | $0.373 \pm 0.028$ | $0.341 \pm 0.023$ | $0.289 \pm 0.008$ |
| Uncoated substrate | $0.617 \pm 0.035$ | $0.562 \pm 0.029$ | $0.532 \pm 0.028$ |

The average COF values of the coatings and the uncoated substrate under different loads during steady-state region are shown in Table 3. By comparing the COFs of the Conventional and the Bimodal, when the applied load is 15 N and 30 N, the average COF of the Bimodal is smaller, and this is because the Bimodal has denser microstructure, larger elastic modulus, and microhardness. Besides, the nano-scale WC particles are dispersedly distributed around the micro-scale WC particles and the CoCr binder phase is completely filled between the WC particles in the Bimodal. The CoCr binder phase has better bond with WC particles in the Bimodal, which is consistent with that of the WC-CoCr coatings in earlier studies [29]. However, when the applied load is 45 N, the average COF of the two is basically the same. The CoCr binder phase is peeled off, a large number of WC particles are pulled out, and the bond of CoCr binder phase and WC particles is destroyed, so the COFs of the two are similar. In addition, it is worth noting that the greater the applied load, the smoother the COF. From Fig. 4(*c*) and Table 3, it can be found that the uncoated AISI 4135 steel also has similar phenomena, but the difference is that the COF of the uncoated substrate under the same condition is greater than that of the coatings.

In order to further quantify the wear data of the coatings and the uncoated substrate under different loads, the wear-rate of the coatings and the uncoated substrate is tested in Fig. 5. As is seen in Fig. 5(*a*), the wear-rate of the Bimodal is lower than that of the Conventional under the same load. Meanwhile, as the load increases, the wear-rate of the coatings increases. The main reason is that the Bimodal has higher microhardness, elastic modulus, and fewer defects, thereby further improving its resistance to sliding friction wear. According to the comparison between Figs. 5(*a*) and 5(*b*), the wear-rate of the uncoated substrate is far greater than that of the coatings, almost two orders of magnitude, which proves

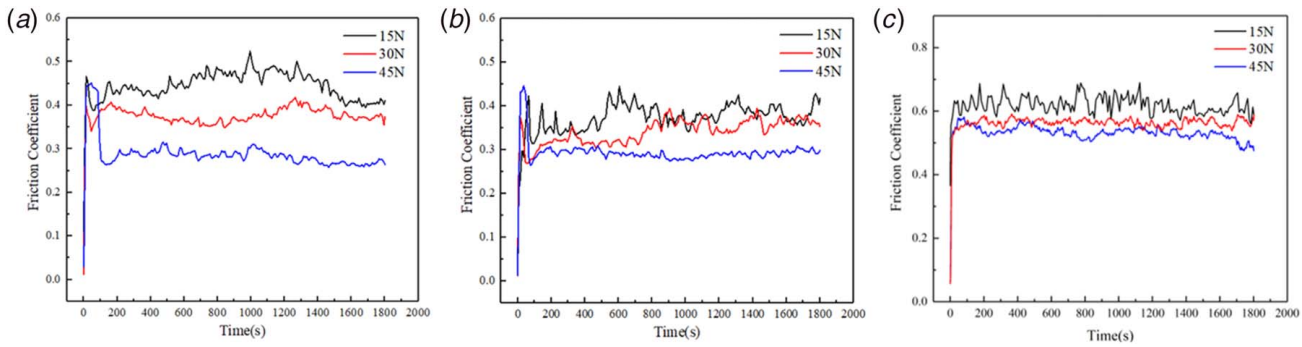


**Fig. 4 COF of the coatings and the uncoated substrate under different loads: (*a*) the Conventional, (*b*) the Bimodal, and (c) the uncoated substrate**

**Table 2 Mechanical properties of the coatings**

| | Bonding strength (MPa) | Fracture toughness ($MPa \cdot m^{1/2}$) | Microhardness ($HV_{0.3}$) | Elastic modulus (GPa) |
|---|---|---|---|---|
| Conventional | $70.7 \pm 6.8$ | $5.80 \pm 0.12$ | $1244 \pm 45$ | $356.5 \pm 18.4$ |
| Bimodal | $72.1 \pm 8.0$ | $5.52 \pm 0.10$ | $1332 \pm 50$ | $397.2 \pm 20.8$ |

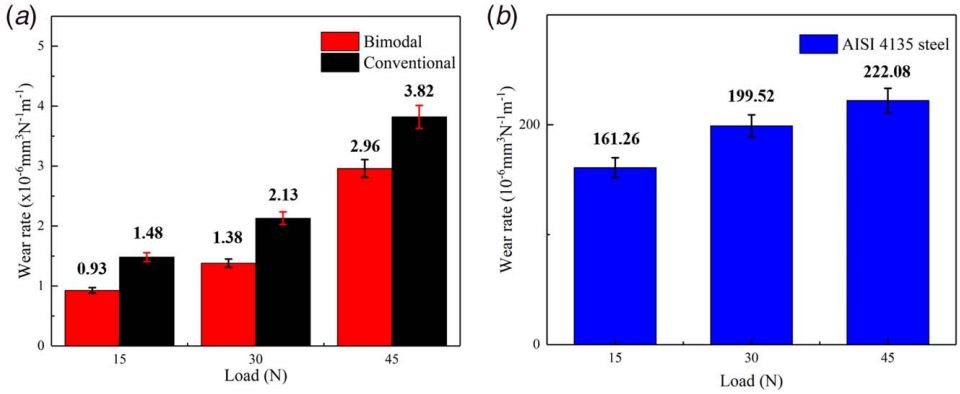


**Fig. 5 Wear-rate of (*a*) the coatings and (*b*) the uncoated substrate under different loads**

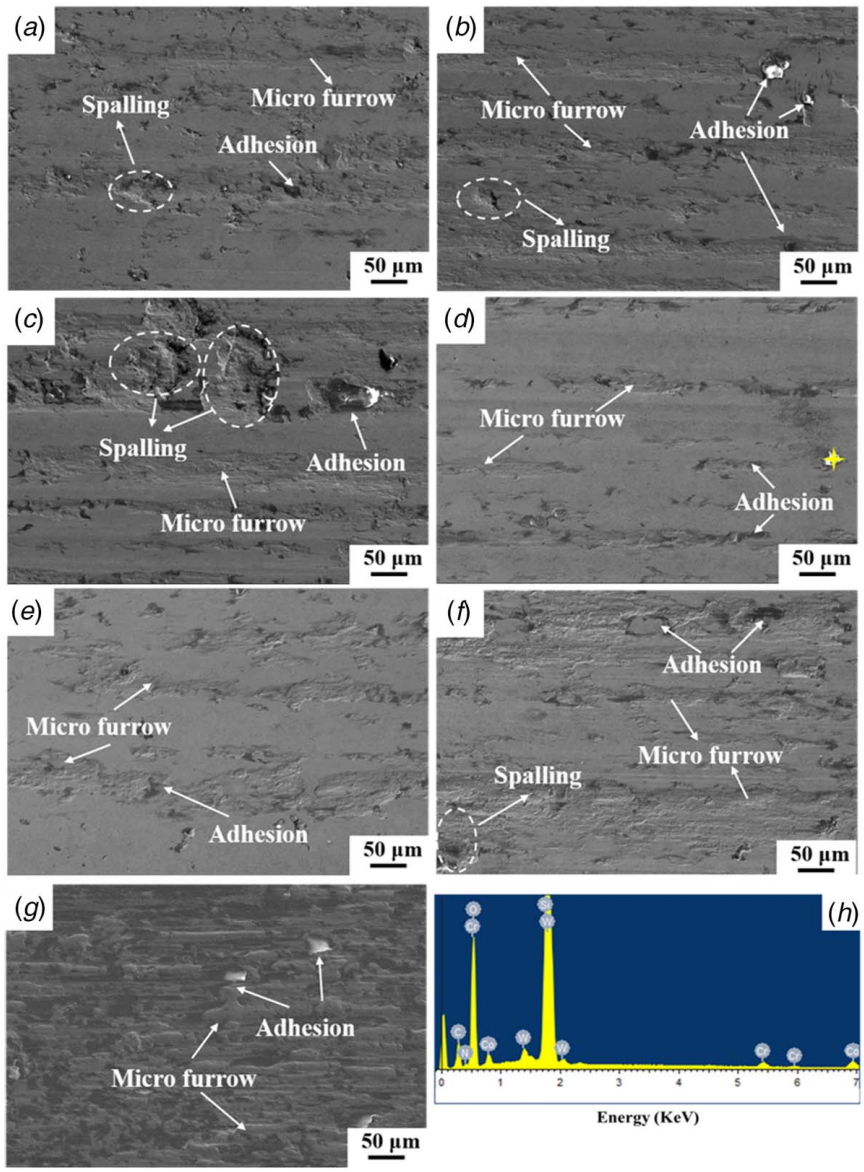


**Fig. 6 SEM images of the worn surfaces of the coatings and the uncoated substrate after sliding wear under different loads: (*a*) the Conventional, 15 N; (*b*) the Conventional, 30 N; (*c*) the Conventional, 45 N; (*d*) the Bimodal, 15 N; (*e*) the Bimodal, 30 N; (*f*) the Bimodal, 45 N; (*g*) the uncoated substrate, 15 N; and (*h*) the EDS point scan at mark of (*d*)**

that the wear resistance of the coating is better than that of the substrate.

The worn surfaces of the coatings and the uncoated substrate after sliding operation under different loads are shown in Fig. 6. It can be seen that the two structural coatings have shallow wear tracks under the load of 15 N, and no obvious plastic deformation occurs (see Figs. 6(*a*) and 6(*d*)). The worn surface of the Conventional is mainly micro furrows and small pits, and slight adhesive wear can also be observed. The worn surface of the Bimodal is mainly micro furrows, and there is also a small amount of adhesive wear. During the sliding friction wear process, the $Si_3N_4$ counterball first wears the CoCr binder phase due to lower microhardness [3,17]. When the binder phase is removed, the WC hard particles are exposed to hinder the relative movement of the counterballs and the coatings, and thus peel off during subsequent sliding friction wear. As a result, WC particles in the coatings are pulled out to form small pits. In addition, part of the exfoliated WC particles continues to move with the counterball, becoming three-body abrasive particles, which exacerbates the wear of the coatings. Besides, the EDS analysis is performed at the mark of Fig. 6(*d*), and its energy spectrum is shown in Fig. 6(*h*) and Table 4. It can be seen that element transfer occurred at the mark, and $Si_3N_4$ on the counterball is transferred to the surface of the coatings [37]. The transferred materials have experienced reaction to generate silicon oxide, which acts as a solid lubricant and reduces the adhesion between the surface of the coatings and the counterball, and subsequently reduces the friction [16,18].

Under the load of 30 N, as is seen in Figs. 6(*b*) and 6(*e*) that the worn surface of the Conventional and the Bimodal show obvious adhesive wear and several ploughed grooves, indicating that the contact depth of the counterball and the coating surface increases with the increase of load, which will increase the adhesive wear. At the same time, the exfoliated WC hard particles continue to act as three-body abrasive particles to exacerbate the wear of coatings [38]. Therefore, the wear failure mechanism of the Conventional and the Bimodal under 30 N load is mainly adhesive wear and three-body wear.

Under the load of 45 N, a large amount of material flaking occurs on the worn surfaces (see Figs. 6(*c*) and 6(*f*)), indicating that a certain degree of fatigue wear has taken place [39]. There are two reasons for the spalling of the coatings. First, large shear stress is generated during the reciprocating friction and wear process, the stress concentration occurs in the subsurface of the coatings. Then, the crack initiation and expansion causes the fatigue wear, which causes the coating to peel off under repeated shear stress. Second, greater contact stress leads to more severe three-body wear [11], and more WC particles are squeezed off the counterball to form small pits during the sliding friction wear. When a large number of small pits are connected to each other, the spalling occurs. In addition, under the load of 45 N, both structural coatings experienced more severe adhesive wear. Therefore, the wear failure forms of both coatings under the 45 N load include fatigue wear in addition to three-body abrasive wear and adhesive wear.

It is worth mentioning that the small pits, micro furrow, and surface spalling of the Bimodal are slighter under the same parameters compared with those of the Conventional, thence the Bimodal has better wear resistance than the Conventional. The better wear resistance of the Bimodal is attributed to its denser microstructure, larger elastic modulus, and microhardness without sacrificing indentation fracture toughness [15,20].

**Table 4 Element contents of at the mark in Fig. 6(*d*)**

| Elements | C | W | Co | Cr | Si | N | O | Total |
|---|---|---|---|---|---|---|---|---|
| Weight percentage | 11.64 | 61.46 | 7.76 | 3.17 | 1.61 | 1.55 | 12.81 | 100 |
| Atomic percentage | 39.32 | 13.56 | 5.34 | 2.48 | 2.32 | 4.50 | 32.48 | 100 |

Figure 6(*g*) shows the worn surface of the uncoated substrate under the load of 15 N. It is obvious that the uncoated substrate has serious abrasive wear and adhesive wear, and it wears more seriously than the coating under the same condition, and the wear failure mechanism is abrasive wear and adhesive wear.

## 4 Conclusion

In this work, the performance between the conventional coating and the bimodal coating is compared, and the effect of loads on the sliding friction and wear performance of the WC-10Co4Cr coatings with conventional structure and bimodal structure was discussed in detail. The conclusions are drawn as follows:

(1) Compared with the conventional coating, the bimodal coating has denser microstructure, lower porosity, and more excellent mechanical properties.
(2) For the effect of load on the COF of the two coatings, the conventional coating and the bimodal coating have shown similar trends that the COFs decrease with the increasing load. Besides, when the applied load is 15 N and 30 N, the average COF of the bimodal coating is smaller and when the applied load is 45 N, the average COF of both coatings is basically the same.
(3) The wear resistance of the WC-10Co4Cr coating is much higher than that of the uncoated substrate. And the wear-rates of the conventional coating and the bimodal coating increase with the increasing load, but the bimodal coating has more excellent wear resistance.
(4) The bimodal coating has better wear resistance than the conventional coating under different loads which is attributed to its denser microstructure, larger elastic modulus, and microhardness without sacrificing indentation fracture toughness. And the two coatings under lower load 15 N and 30 N only exhibit abrasive and slightly adhesive wear mechanism, while in the highest load application of 45 N, additional mechanism which is fatigue is detected and causes flaking of the coating.

## Acknowledgment

This project is supported by the National Natural Science Foundation of China (Grant Nos. 41772389 and 41872183), the Pre-Research Program in National 13th Five-Year Plan (Grant No. 61409230603), the Tribology Science Fund of State Key Laboratory of Tribology (Grant No. SKLTKF19B12), and the Fundamental Research Funds for Central Universities (Grant No. 2652019069).

## Conflict of Interest

There are no conflicts of interest.

## References

[1] Liu, Y. L., Cheng, J., Yin, B., Zhu, S. Y., Qiao, Z. H., and Yang, J., 2017, "Study of the Tribological Behaviors and Wear Mechanisms of WC-Co and WC-$Fe_3Al$ Hard Materials Under Dry Sliding Condition," Tribol. Int., **109**, pp. 19–25.
[2] Sathisha, C. H., Ravikumar, B. N., Anand, K., and Shalini, T., 2016, "Elevated Temperature Fretting Wear Behavior of Cobalt-Based Alloys," ASME J. Tribol., **138**(3), p. 031601.
[3] Wang, H. B., Wang, X. Z., Song, X. Y., Liu, M. M., and Liu, X. W., 2015, "Sliding Wear Behavior of Nanostructured WC-Co-Cr Coatings," Appl. Surf. Sci., **355**, pp. 453–460.
[4] Ma, N., Guo, L., Cheng, Z. X., Wu, H. T., Ye, F. X., and Zhang, K. K., 2014, "Improvement on Mechanical Properties and Wear Resistance of HVOF Sprayed WC-12Co Coatings by Optimizing Feedstock Structure," Appl. Surf. Sci., **320**, pp. 364–371.
[5] Chen, G. Q., Zhang, B. G., Wu, Z. Z., Shu, X., and Feng, J. C., 2017, "Microstructure Transformation and Crack Sensitivity of WC-Co/Steel Joint Welded by Electron Beam," Vacuum, **139**, pp. 26–32.

[6] Zhu, X. P., Du, P. C., Meng, Y., Lei, M. K., and Guo, D. M., 2017, "Solution to Inverse Problem of Manufacturing by Surface Modification With Controllable Surface Integrity Correlated to Performance: A Case Study of Thermally Sprayed Coatings for Wear Performance," ASME J. Tribol., **139**(6), p. 061604.
[7] Hong, S., Wu, Y. P., Gao, W. W., Zhang, J. F., Zheng, Y. G., and Zheng, Y., 2018, "Slurry Erosion-Corrosion Resistance and Microbial Corrosion Electrochemical Characteristics of HVOF Sprayed WC-10Co-4Cr Coating for Offshore Hydraulic Machinery," Int. J. Refract. Met. Hard. Mater., **74**, pp. 7–13.
[8] Zhou, Y.-K., Liu, X.-B., Kang, J.-J., Yue, W., Qin, W.-B., Ma, G.-Z., Fu, Z.-Q., Zhu, L.-N., She, D.-S., Wang, H.-D., Liang, J., Weng, W., and Wang, C.-B., 2020, "Corrosion Behavior of HVOF Sprayed WC-10Co4Cr Coatings in the Simulated Seawater Drilling Fluid Under High Pressure," Eng. Failure Anal., **109**, p. 104338.
[9] Liu, X. B., Kang, J. J., Yue, W., Fu, Z. Q., Zhu, L. N., She, D. S., Liang, J., and Wang, C. B., 2019, "Performance Evaluation of HVOF Sprayed WC-10Co4Cr Coatings Under Slurry Erosion," Surf. Eng., **35**(9), pp. 816–825.
[10] Zhu, L. N., Wang, C. B., Wang, H. D., Xu, B. S., Zhuang, D. M., Liu, J. J., and Li, G. L., 2012, "Microstructure and Tribological Properties of $WS_2$/$MoS_2$ Multilayer Films," Appl. Surf. Sci., **258**(6), pp. 1944–1948.
[11] Lin, L., Li, G. L., Wang, H. D., Kang, J. J., Xu, Z. L., and Wang, H. J., 2015, "Structure and Wear Behavior of NiCr-$Cr_3C_2$ Coatings Sprayed by Supersonic Plasma Spraying and High Velocity Oxy-Fuel Technologies," Appl. Surf. Sci., **356**, pp. 383–390.
[12] Kamdi, Z., Shipway, P. H., Voisey, K. T., and Sturgeon, A. J., 2011, "Abrasive Wear Behaviour of Conventional and Large-Particle Tungsten Carbide-Based Cermet Coatings as a Function of Abrasive Size and Type," Wear, **271**(9–10), pp. 1264–1272.
[13] Wang, Q., Chen, Z. H., and Ding, Z. X., 2009, "Performance of Abrasive Wear of WC-12Co Coatings Sprayed by HVOF," Tribol. Int., **42**(7), pp. 1046–1051.
[14] Basak, A. K., Celis, J. P., Ponthiaux, P., Wenger, F., Vardavoulias, M., and Matteazzi, P., 2012, "Effect of Nanostructuring and Al Alloying on Corrosion Behaviour of Thermal Sprayed WC-Co Coatings," Surf. Coat. Technol., **558**(16), pp. 377–385.
[15] Guilemany, J. M., Dosta, S., Nin, J., and Miguel, J. R., 2005, "Study of the Properties of WC-Co Nanostructured Coatings Sprayed by High-Velocity Oxyfuel," J. Therm. Spray Technol., **14**(3), pp. 405–413.
[16] Mi, P. B., Wang, T., and Ye, F. X., 2017, "Influences of the Compositions and Mechanical Properties of HVOF Sprayed Bimodal WC-Co Coating on Its High Temperature Wear Performance," Int. J. Refract. Met. Hard. Mater., **69**(3), pp. 158–163.
[17] Lekatou, A., Sioulas, D., Karantzalis, A. E., and Grimanelis, D., 2015, "A Comparative Study on the Microstructure and Surface Property Evaluation of Coatings Produced From Nanostructured and Conventional WC–Co Powders HVOF-Sprayed on Al7075," Surf. Coat. Technol., **276**, pp. 539–556.
[18] Gao, Y., Gao, C. Q., Gao, J. Y., and Cai, L., 2019, "Comparison of the Mechanical and Wear-Resistant Properties of WC-13Ni4Cr and WC-10Co4Cr Coatings Obtained by Detonation Spraying," J. Therm. Spray Tech., **28**(4), pp. 851–861.
[19] Ji, G. C., Wang, H. T., Chen, X., Bai, X. B., Dong, Z. X., and Yang, F. G., 2013, "Characterization of Cold-Sprayed Multimodal WC-12Co Coating," Surf. Coat. Technol., **235**, pp. 536–543.
[20] Wang, Q., Chen, Z. H., Li, L. X., and Yang, G. B., 2012, "The Parameters Optimization and Abrasion Wear Mechanism of Liquid Fuel HVOF Sprayed Bimodal WC–12Co Coating," Surf. Coat. Technol., **206**(8–9), pp. 2233–2241.
[21] Konyashin, I., Ries, B., and Lachmann, F., 2010, "Near-Nano WC–Co Hardmetals: Will They Substitute Conventional Coarse-Grained Mining Grades?," Int. J. Refract. Met. Hard. Mater., **28**(4), pp. 489–497.
[22] Zhao, S. X., Song, X. Y., Wei, C. B., Zhang, L., Liu, X. M., and Zhang, J. X., 2009, "Effects of WC Particle Size on Densification and Properties of Spark Plasma Sintered WC-Co Cermet," Int. J. Refract. Met. Hard. Mat., **27**(6), pp. 1014–1018.
[23] Wang, H. B., Yang, T., Song, X. Y., Liu, X. M., Wang, X. Z., and Wu, X., 2017, "Wear Resistance Enhancement of Bimodal-Grained Cemented Carbide Coating," Surf. Coat. Technol., **309**, pp. 759–766.
[24] Tang, L., Kang, J. J., He, P. F., Ding, S. Y., Chen, S. Y., Liu, M., Xiong, Y. C., Ma, G. Z., and Wang, H. D., 2019, "Effects of Spraying Conditions on the Microstructure and Properties of NiCrBSi Coatings Prepared by Internal Rotating Plasma Spraying," Surf. Coat. Technol., **374**, pp. 625–633.
[25] Evans, A. G., and Wilshaw, T. R., 1976, "Quasi-Static Solid Particle Damage in Brittle Solids—I. Observations Analysis and Implications," Acta Metall., **24**(10), pp. 939–956.
[26] Geng, Z., Li, S., Duan, D. L., and Liu, Y., 2015, "Wear Behaviour of WC–Co HVOF Coatings at Different Temperatures in Air and Argon," Wear, **330**, pp. 348–353.
[27] Zhao, X. Q., Zhou, H. D., and Chen, J. M., 2006, "Comparative Study of the Friction and Wear Behavior of Plasma Sprayed Conventional and Nanostructured WC-12%Co Coatings on Stainless Steel," Mat. Sci. Eng. A—Struct., **431**(1–2), pp. 290–297.
[28] Su, J., Kang, J.-J., Yue, W., Ma, G.-Z., Fu, Z.-Q., Zhu, L.-N., She, D.-S., Wang, H.-D., and Wang, C.-B., 2019, "Comparison of Tribological Behavior of Fe-Based Metallic Glass Coatings Fabricated by Cold Spraying and High Velocity Air Fuel Spraying," J. Non-Cryst. Solids, **552**, p. 119582.
[29] Guilemany, J. M., Dosta, S., and Miguel, J. R., 2006, "The Enhancement of the Properties of WC-Co HVOF Coatings Through the Use of Nanostructured and Microstructured Feedstock Powders," Surf. Coat. Technol., **201**(3–4), pp. 1180–1190.
[30] Park, S. Y., Kim, M. C., and Park, C. G., 2007, "Mechanical Properties and Microstructure Evolution of the Nano WC–Co Coatings Fabricated by Detonation Gun Spraying With Post Heat Treatment," Mat. Sci. Eng. A—Struct., **449**, pp. 894–897.
[31] Sudaprasert, T., Shipway, P. H., and McCartney, D. G., 2003, "Sliding Wear Behaviour of HVOF Sprayed WC–Co Coatings Deposited With Both Gas-Fuelled and Liquid," Wear, **255**, pp. 943–949.
[32] Stewart, D. A., Shipway, P. H., and McCartney, D. G., 2000, "Microstructural Evolution in Thermally Sprayed WC–Co Coatings: Comparison Between Nanocomposite and Conventional Starting Powders," Acta Mater., **48**, pp. 1593–1604.
[33] Wang, Q., Zhang, S. Y., Cheng, Y. L., Xiang, J., Zhao, X. Q., and Yang, G. B., 2013, "Wear and Corrosion Performance of WC-10Co4Cr Coatings Deposited by Different HVOF and HVAF Spraying Processes," Surf. Coat. Technol., **218**, pp. 127–136.
[34] Yin, B., Zhou, H. D., Yi, D. L., Chen, J. M., and Yan, F. Y., 2010, "Microsliding Wear Behaviour of HVOF Sprayed Conventional and Nanostructured WC–12Co Coatings at Elevated Temperatures," Surf. Eng., **26**(6), pp. 469–477.
[35] Qin, W. B., Li, J. S., Liu, Y. Y., Kang, J. J., Zhu, L. N., Shu, D. F., Peng, P., She, D. S., Meng, D. Z., and Li, Y. S., 2019, "Effects of Grain Size on Tensile Property and Fracture Morphology of 316L Stainless Steel," Mater. Lett., **254**, pp. 116–119.
[36] Hong, S., Wu, Y. P., Wang, B., Zhang, J. F., Zheng, Y., and Qiao, L., 2017, "The Effect of Temperature on the Dry Sliding Wear Behavior of HVOF Sprayed Nanostructured WC-CoCr Coatings," Ceram. Int., **43**(1), pp. 458–462.
[37] Liu, Y., Liu, W., Ma, Y., Meng, S., Liu, C., Long, L., and Tang, S., 2017, "A Comparative Study on Wear and Corrosion Behaviour of HVOF- and HVAF-Sprayed WC–10Co–4Cr Coatings," Surf. Eng., **33**(1), pp. 63–71.
[38] Karuppusamy, P., Lingadurai, K., and Sivananth, V., 2019, "To Study the Role of WC Reinforcement and Deep Cryogenic Treatment on AZ91 MMNC Wear Behavior Using Multilevel Factorial Design," ASME J. Tribol., **141**(4), 041608.
[39] Piao, Z. Y., Xu, B. S., Wang, H. D., and Yu, X. X., 2019, "Rolling Contact Fatigue Behavior of Thermal Sprayed Coating: A Review," Crit. Rev. Solid State Mater. Sci., **45**(6), pp. 1–28.